Performance of the Fourier Transform Reconstructor for the European Extremely Large Telescope

I. Montilla[a], M. Reyes[a], M. Le Louarn[b], J. G. Marichal-Hernández[c], J. M. Rodríguez-Ramos[c], L. F. Rodríguez-Ramos[a]
[a]Instituto de Astrofísica de Canarias, C/ Vía Láctea s/n, La Laguna, Tenerife, Spain;
[b]European Southern Observatory, Karl Schwarzschild Strasse 2, Garching bei München, Germany
[c]Universidad de La Laguna, Tenerife, Spain

ABSTRACT

The forthcoming Extremely Large Telescopes, and the new generation of Extreme Adaptive Optics systems, carry on a boost in the number of actuators that makes the real-time correction of the atmospheric aberration computationally challenging. It is necessary to study new algorithms for performing Adaptive Optics at the required speed. Among the last generation algorithms that are being studied, the Fourier Transform Reconstructor (FTR) appears as a promising candidate. Its feasibility to be used for Single-Conjugate Adaptive Optics has been extensively proved by L. Poyneer[1]. As part of the activities supported by the ELT Design Study (European Community's Framework Programme 6) we have studied the performance of this algorithm applied to the case of the European ELT, in two different cases: single-conjugate and ground-layer adaptive optics and we are studying different approaches to apply it to the more complex multi-conjugate case. The algorithm has been tested on ESO´s OCTOPUS software, which simulates the atmosphere, the deformable mirror, the sensor and the closed-loop control. The performance has been compared with other algorithms as well as their response in the presence of noise and with various atmospheric conditions. The good results on performance and robustness, and the possibility of parallelizing the algorithm (shown by Rodríguez-Ramos and Marechal-Hernández) make it an excellent alternative to the typically used Matrix-Vector Multiply algorithm.

Keywords: adaptive optics, reconstruction algorithms, fourier techniques

1. INTRODUCTION

Fourier-domain methods have a high potential for AO systems. They take advantage of the FFT (Fast-Fourier Transform) which decreases the complexity from $O(N^4)$, which is the complexity for the Matrix-Vector Multiply (MVM) method, to $O(N^2 \log N)$. The Fourier Transform Reconstructor (FTR) is being extensively studied. Our starting point was a revision of the method, for Single Conjugate Adaptive Optics (SCAO) and Ground Layer Adaptive Optics (GLAO). We performed local simulations, under static conditions, and once they gave a successful response, the programs were integrated in the end-to-end Adaptive Optics simulator at the European Southern Observatory, OCTOPUS, to test the performance of the algorithm and compare it with the other reconstructors studied in the European-Extremely Large Telescope (E-ELT) Algorithms and Reconstruction Work Package. The integration campaign had an excellent result, and the impact of many parameters was evaluated, such as atmospheric turbulence, star magnitude, closed-loop gain, wind speed and actuator shift, for the SCAO case using 84x84 subapertures for a telescope diameter of 42 m. This paper summarizes the tests performed at ESO, to integrate the FTR code with OCTOPUS, and to check the performance of the reconstructor in order to compare it with the other reconstruction methods (the Fractal Iterative Method, FrIM, and the MVM, comparison is presented in a different paper[2]). First, in Section 2 we describe very briefly the E-ELT, its design and scientific goals. In Section 3 we explain the basic principles of the reconstruction method, to focus on the results of the tests in Section 4. Since the main reason to study this method is its capability of performing real-time correction with large numbers of actuators, in Section 5 we show a possible architecture to parallelize the algorithm and present some figures on the latency that it would have using this architecture. We finish with some conclusions in Section 6.

2. THE EUROPEAN EXTREMELY LARGE TELESCOPE

The E-ELT is a project jointly funded by the European Southern Observatory (ESO) and the European Community. The preliminary design of the facility started in 2007, and the goal is to have the E-ELT Observatory operational around 2015. A large group of European Institutes are developing critical studies and technologies to make it possible. The latest proposed design consists of a telescope with a diameter of up to 42 m, and an f-ratio of 15. The work presented in this paper is part of the European ELT Design Study.

The E-ELT scientific goals have been described by Hook et al.[3], and among the most important scientific cases we can find the direct detection of earth-like planets in extrasolar systems, the study of protoplanetary disks and galaxy formation, observing high-redshift galaxies and studying the re-ionization of the early universe. All of them require not only a large collecting area, but also a good spatial resolution. It is essential to build any ELT with a powerful Adaptive Optics (AO) system to unleash all its scientific potential. High performance AO is a critical requirement for any ELT. For example, for the detection of exo-earth planets, a high Strehl ratio of 70%-90% will be required, and to study the inner region of circumstellar disks, diffraction–limited resolution is needed. The computational burden to obtain such correction at the required speed is too large for the classical AO algorithms, demanding faster high-performance algorithms to be developed.

3. FOURIER TRANSFORM RECONSTRUCTOR: BASIC PRINCIPLES

The wavefront reconstruction method using a Discrete Fourier Transform was first proposed by Freischlad and Koliopoulos[4], and later adapted by Poyneer[1] for use on the Fried geometry. It basically consists in reconstructing the wavefront in Fourier space, by applying a certain filter to the Fourier transform of the gradients of the subapertures sampled by the detector. The gradients provided by the detector are $s_x[m,n]$ and $s_y[m,n]$, that in the case of the Shack-Hartmann geometry are:

$$s_x[m,n] = \tfrac{1}{2}(\phi[m,n+1]-\phi[m,n]+\phi[m+1,n+1]-\phi[m+1,n]) \tag{1}$$

$$s_y[m,n] = \tfrac{1}{2}(\phi[m+1,n]-\phi[m,n]+\phi[m+1,n+1]-\phi[m,n+1]) \tag{2}$$

Their Fourier transforms are $S_x[k,l]$ and $S_y[k,l]$. The reconstructed wavefront in the Fourier space is:

$$\hat{\phi}[k,l] = \begin{cases} 0, & k,l = 0, N/2 \\ F_x[k,l]S_x[k,l] + F_y[k,l]S_y[k,l], & else \end{cases} \tag{3}$$

where $F_x[k,l]$ and $F_y[k,l]$ are the coefficients of the filter derived for a given geometry. The coefficients when using the Fried filter for the Shack-Hartmann geometry are:

$$F_x[k,l] = \frac{\left(e^{\left(-j2\pi k/N\right)}-1\right)\left(e^{\left(-j2\pi l/N\right)}+1\right)}{T[k,l]}, \tag{4}$$

$$F_y[k,l] = \frac{\left(e^{\left(-j2\pi l/N\right)}-1\right)\left(e^{\left(-j2\pi k/N\right)}+1\right)}{T[k,l]}, \tag{5}$$

with

$$T[k,l] = 8\left[\sin^2\left(\pi k/N\right)\cos^2\left(\pi l/N\right)+\sin^2\left(\pi l/N\right)\cos^2\left(\pi k/N\right)\right]. \tag{6}$$

In a real system gradients are only available typically on a circular aperture, and the measurements have to be extended to a rectangular grid and some periodicity has to be imposed to the extended data. This paper does not focus on these subjects, so for more information on extension methods, as well as for the details on the filter applied when using Fried geometry, we refer to Poyneer et al.[1]. In our simulations we were interested in obtaining the commands that had to be sent to the actuators of the deformable mirror that actually corrects the atmospheric turbulence. These commands are:

$$C[m,n] = IFT\left\{\frac{\hat{\phi}[k,l]}{FT[I(m,n)]}\right\} \tag{7}$$

where $I(m,n)$ is the influence function of the actuators.

4. PERFORMANCE TESTS: OCTOPUS SIMULATIONS

OCTOPUS is the end-to-end Adaptive Optics simulator of the European Southern Observatory[5]. It simulates the atmosphere, the deformable mirror, the sensor and, in our case, also the closed-loop control. The simulated sensor samples the incoming wavefront and generates the centroids that are used by our code to reconstruct the wavefront. The computed commands for the deformable mirror are sent back to OCTOPUS, which performs the control and closes the loop.

The tests that we present in this section have been done with the E-ELT model, using a telescope diameter of 42 m, with a central obscuration of 28%. The pupil is circular, and segmentation co-phasing errors are neglected. The wavefront-sensor assumes a squared 84x84 subaperture geometry. This gives a subaperture size on the sky of 50 cm. There are 5040 active subapertures across the telescope pupil (active means that they are not behind the central obstruction).

The deformable mirror geometry consists on a grid of 85x85 actuators. The total amount of active actuators is 5402. In all the tests we used the Shack-Hartmann geometry, placing the actuators at the corners of the subapertures, and the Fried filter for the reconstruction. Further tests using the Hudgin filter are planned.

4.1 Single-conjugate adaptive optics simulations

The complete block diagram of the SCAO simulations can be seen in Fig. 1. The default configuration we used for the simulations is:

- Influence function= bilinear spline, in OCTOPUS and FTR code.
- Shack-Hartmann gain=1
- rate = 1 KHz (for phase screens displacement evaluation)
- #iterations= 50
- Delay= 2 frames
- No RON is considered
- Photon noise is considered

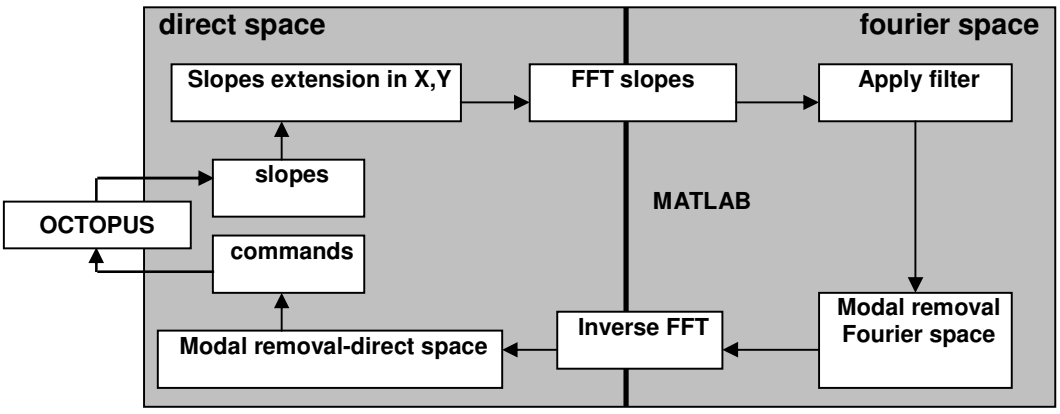

Fig. 1: SCAO block diagram

First we have tested the dependency of the performance on the star magnitude, setting the following configuration:

- Wind speed ~3 ms
- r_0= 0.13 m

The star magnitude is scanned, optimizing the closed-loop gain. Tests were performed for 1000, 100, 10, and 1 ph/subaperture/cycle. The results are plotted in Fig. 2, where we have plotted the K-band Strehl ratio vs. the iteration number. For a magnitude of 1000 ph/subaperture/cycle, using a gain of 0.45, the Strehl is higher than 80%. For a magnitude of 100 ph/subaperture/cycle, the performance is a bit degraded and the Strehl is a bit lower than 80%. For 10 ph/subaperture/cycle the Strehl is larger than 70%. Finally, for a magnitude of 1 ph/subaperture/cycle, the Strehl converges to almost 50%. It seems that the FTR outperforms both FriM and MVM at magnitudes corresponding to faint sources (10 ph/subaperture/cycle and 1 ph/subaperture/cycle). This is particularly interesting because it brings on the opportunity of using fainter objects as guide stars.

Following we performed some tests to determine which level of turbulence was the maximum that the algorithm was able to correct. We tested different values of r_0, while using the following configuration:

- 1000 ph/subaperture/cycle
- Wind speed ~3 ms
- CL gain = 0.6

The results are plotted in Fig. 3. For an r_0 of 13 cm, the K-band Strehl is over 80%, while it decreases to around 71% for a seeing of 10 cm and to 52% for 7 cm. For a very bad case, a seeing of 5 cm, the K-band Strehl still converges but it is 30%.

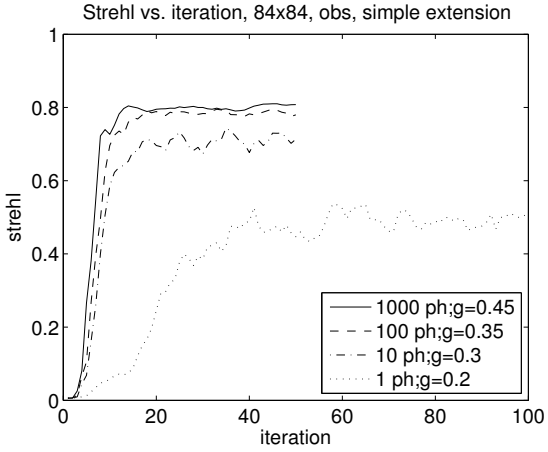

Fig. 2: Strehl vs. iteration number for different magnitudes

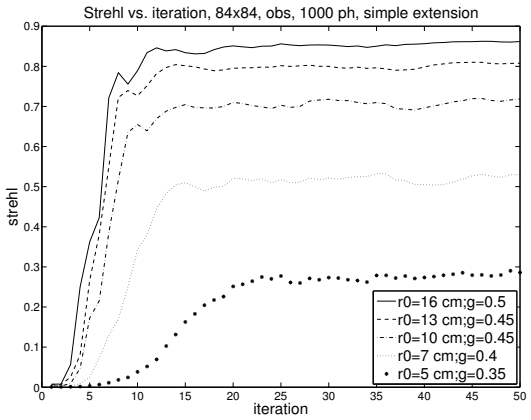

Fig. 3: Strehl vs. iteration number for different values of r_0

We also did tests to check the behavior of the performance for different coherence times. One of the first conclusions that we can reach from this simulation is that for a coherence time larger than 3 ms the performance is limited due to the number of actuators, so beyond this limit a larger coherence time does not imply a better performance. Below this limit we see a degradation of the performance for shorter coherence times. The lower limit corresponds to 1 ms, which Strehl is down to 60%.

Finally, we have performed simulations for different actuators displacements to test how robust is the algorithm. The goal is to test what happens to the performance when the actuators are not placed where they should be. Each subaperture has 16 pixels, and we shifted the position of the actuators 2, 4, 6 and 8 pixels, without giving this information to the algorithm. We realized that the response was good until there was a displacement of 8 pixels, or half a subaperture. Therefore, the algorithm seems to be very robust to face this kind of problem.

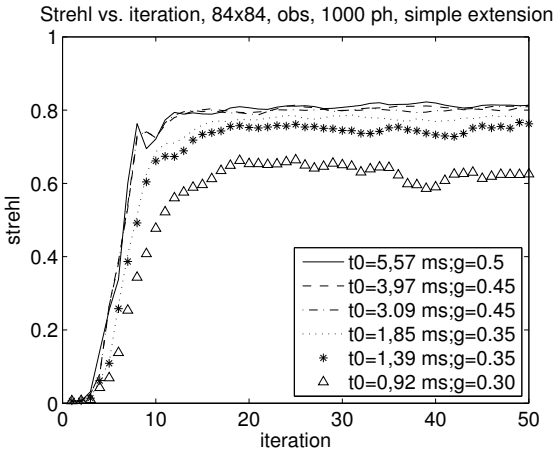

Fig. 4: Strehl vs. iteration number for different values of the coherence time.

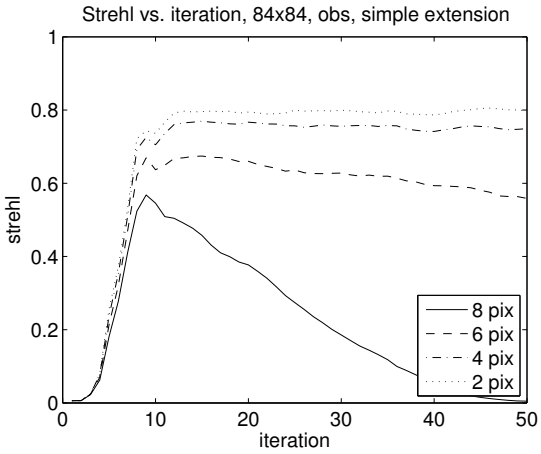

Fig. 5: Strehl vs. iteration number for different actuators misregistrations

4.2 Ground-layer adaptive optics simulations

The complete block diagram of the FTR applied to GLAO compensation, from centroids to actuator commands, is shown in Fig. 6. As can be seen, the main difference with regard to the SCAO case is that there is slope information from many guide stars. The average from the slopes of the different guide stars is calculated and used as input for the FTR algorithm. The rest of the diagram is similar to the SCAO case.

In the simulations done with OCTOPUS, there are 4 laser guide stars (LGS's) in a circle of 1.5 arcmin. The result is plotted in Fig. 7. The Strehl is very low, and we can understand why if we compare the results with the Strehl from our local simulations. In our local simulations, we placed 4 natural guide stars (NGS's) in a 1.5 arcmin circle. The Strehl after 50 iterations was ~16%. Then we placed 4 LGS's in a 1.5 arcmin circle, and the Strehl went down to ~3%. In the OCTOPUS simulations, the Strehl was 4%. This seems mainly due to the fact of using laser guide stars and not natural guide stars. The LGS's are placed at a height of 90 km, but in the reconstruction they are considered to be at infinity. The cone effect in the telescope pupil cannot be neglected.

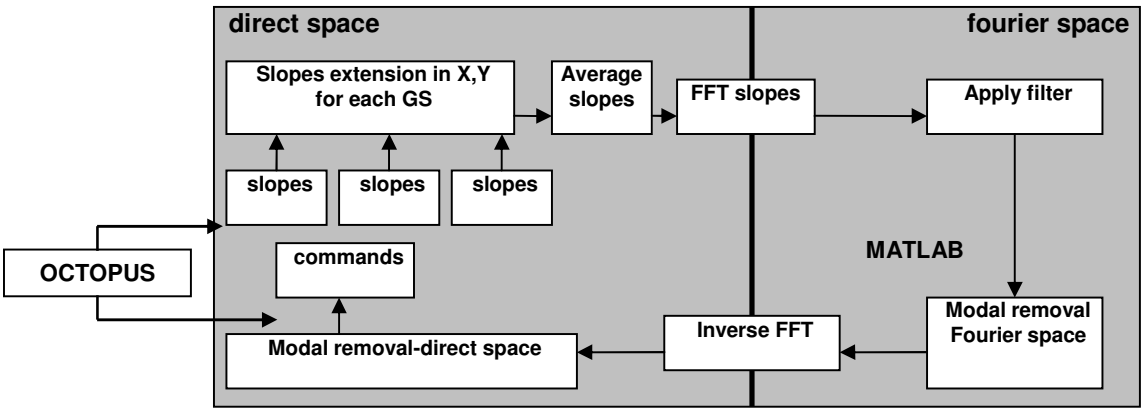

Fig. 6: GLAO block diagram

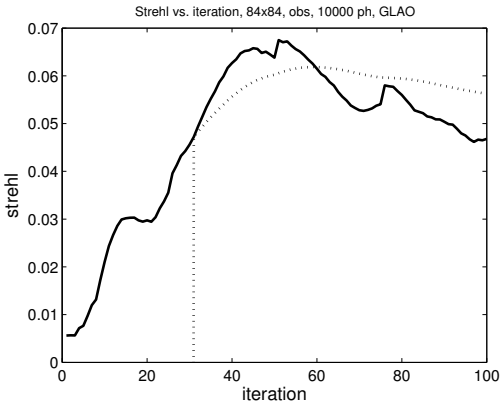

Fig. 7: Short exposure and long exposure (dotted line) strehl vs. iteration number for GLAO at OCTOPUS

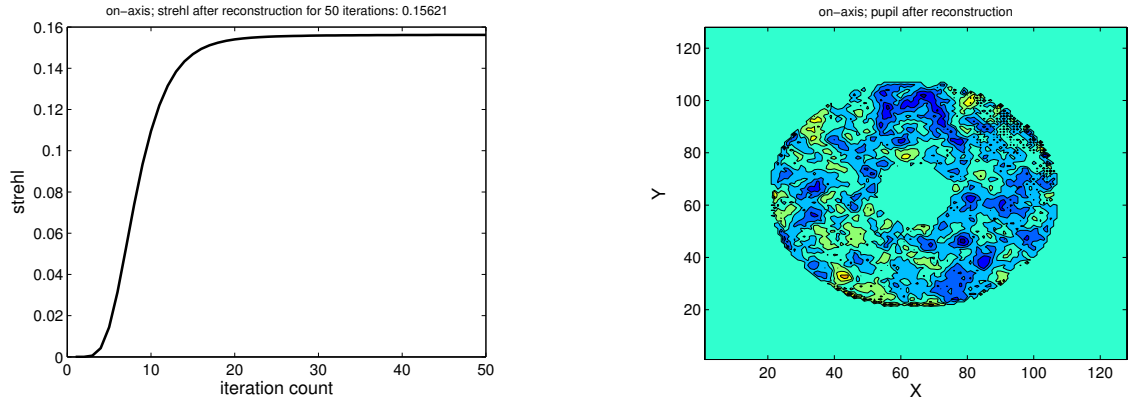

Fig. 8: Strehl vs. iteration number (left) and pupil after reconstruction (right) for the GLAO case in the local simulations with NGS's.

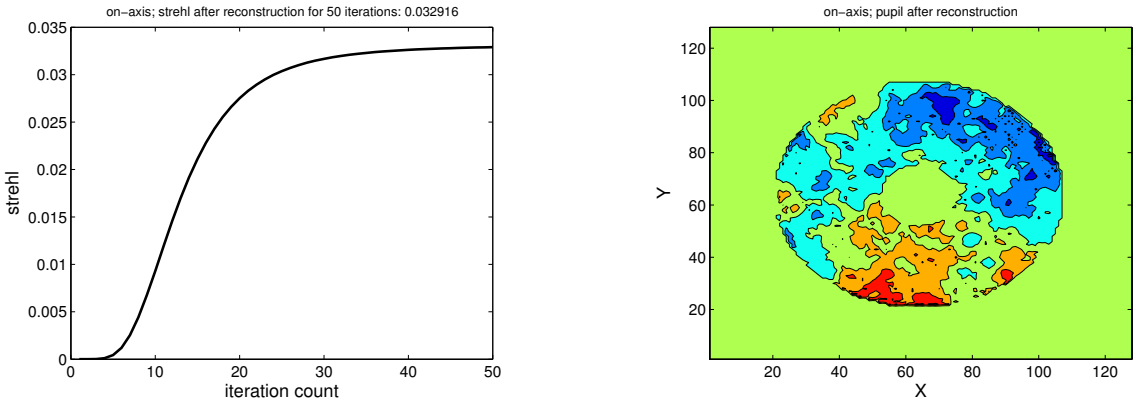

Fig. 9: Strehl vs. iteration number (left) and pupil after reconstruction (right) for the GLAO case in the local simulations with LGS's.

5. REAL-TIME COMPUTATION

The FFT should not be considered a black box[6]. It can be decomposed in smaller tasks, it can be parallelized and it has been parallelized in several ways. There is a large research on that field (see [6] and [7]). The algorithm is parallelized in one way or another, depending on the configuration of the detector. What we present in this section is not strictly a parallelization, in the sense of using several processors, because what we assumed is that we have only one processor, but it computes operations at the same time as it reads the data from the detector. In [8], the control matrix of the MVM algorithm was partitioned in half the number of subapertures across the aperture to allow for parallelizing. The columns of the control matrix where multiplied using a parallelized decomposition. In this way, the operations were performed at the same time as the columns were read, two by two, and the RTC latency corresponded to the operations taken to compute the last two columns:

$$N_{op}^{MVM} = 2 \cdot \left(N^2 - N\right) \cdot N^2 = 2 \cdot \left(N^4 - N^3\right), \tag{8}$$

$$N_{op}^{MVMpl} = \frac{N_{op}^{MVM}}{N/2}, \tag{9}$$

To compare both cases, we proceed in a similar way with the FTR algorithm. First, we decompose the 2D FFT's into 1D FFT's, using the row-column method[6]. Each 1D FFT is decomposed and handled as a radix-2 FFT[9]. With this approach the computation of an N-point DFT is replaced by that of two DFT's of length N/2 plus N additions and N/2 multiplications. A systematic application of this method computes the DFT of length 2t in t=log2N stages, each stage converting 2i DFT's of length 2t-i into 2i+1 DFT's of length 2t-i-1 at the cost of N additions and N/2 multiplications. Summarizing, the number of operations, to compute a DFT of length N by the radix-2 FFT algorithm is:

$$N_{op} = 3\frac{N}{2}\log_2 N, \tag{10}$$

The computation structure is shown in Fig. 10. It can be seen that there are log2N stages, and in each stage the elements are computed 2-by-2 in what is called a butterfly, so there are N/2 butterflies each one performing 3 operations in each stage.

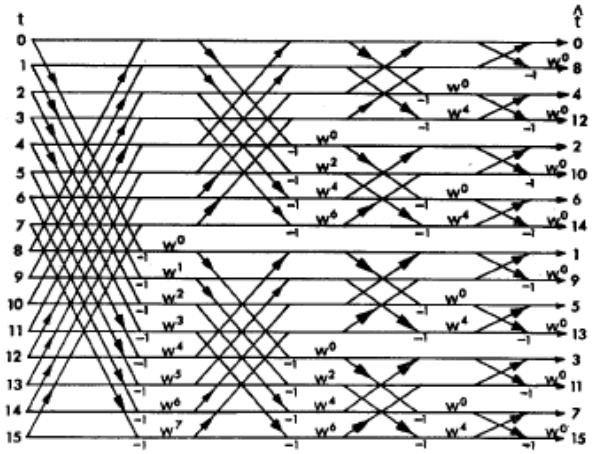

Fig. 10: flow graph representation of a 16-point FFT algorithm

This allows performing the 1D FFT's of the columns at the same time they are being read, as with the MVM algorithm. For the rows, we can compute part of the butterflies, but not all of them since we are lacking the last two columns. To calculate the latency, we should proceed somehow in a way similar to the pruning technique[10]. We cannot perform the last butterfly of the first stage; this prevents us of performing 2 butterflies in the second stage, 4 in the third stage and so on. For each row, the number of operations that we cannot perform until we read the last two columns is:

$$N_{op} = 3 \sum_{j=0}^{\log_2 N-1} 2^j \,, \tag{11}$$

So for each NxN decomposed 2D FFT, the number of multiplications that still have to be performed after reading the two last columns is:

$$N_{op}^{2DFFT} = N \cdot \sum_{j=0}^{\log_2 N-1} 2^j + N \cdot \log_2(N) \tag{12}$$

These are complex multiplications; each one corresponds to three real multiplications[6]. There are 2 forward 2D FFT's, therefore, for the FTR algorithm, the RTC latency corresponding to the time taken to compute the forward FFT's of the last two columns, plus the time to filter and compute the complete Inverse Fourier Transform, will be:

$$N_{op}^{FTRpl} = \frac{\frac{5}{4}N^2 + 6N^2}{N/2} + 2 \cdot \left(3N \cdot \sum_{j=0}^{\log_2 N-1} 2^j + 3N \cdot \log_2(N) \right) + 4N^2 + 3 \cdot N^2 \cdot \log_2(N) \tag{13}$$

But since the forward 2D FFT's are real-valued, we can also apply the approach used by Marichal-Hernández et al.[7], also explained in[6], and compute them together as if they were the real and the imaginary part of a complex Fourier Transform, using the symmetry property of the real-valued FFT. The number of operations is almost divided by two, being reduced to:

$$N_{op}^{FTRpl} = \frac{\frac{5}{4}N^2 + 6N^2}{N/2} + \left(3 \cdot N \cdot \sum_{j=0}^{\log_2 N-1} 2^j + 3 \cdot N \cdot \log_2(N) + \frac{4N^2}{N/2} \right) + 4N^2 + 3 \cdot N^2 \cdot \log_2(N) \tag{14}$$

We have represented in Fig. 11 the number of operations vs. the number of subapertures across the aperture for the two algorithms parallelized. For 210x210 subapertures, the parallelized FTR algorithm is ~30 times faster than the MVM algorithm. Most of the latency is due to the inverse FFT, which is not parallelized because we are using only one processor, and we have to wait until the 2 direct FFT's are computed. This explains why the number of operations of the MVM decreases more than the number of operations of the FTR. Using several processors instead of one should be an advantage for the FTR.

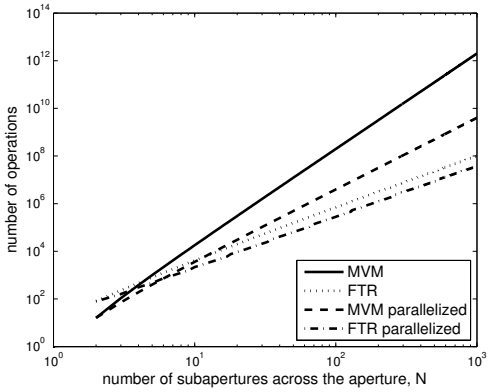

Fig. 11: number of operations vs. number of subapertures

6. CONCLUSIONS AND FUTURE WORK

We can conclude that the results of these first tests are promising. The algorithm seems to have a very good performance and a very robust response. In general, the performance was degraded only for the most extreme conditions (a star magnitude of 1 ph.subaperture^{-1}cycle^{-1}, a coherence time smaller than 1 ms, or an actuator misregistration of half a subaperture). Slight degradations of the conditions do not seem to affect its performance. An interesting result is the good response of the FTR at magnitudes corresponding to faint sources (10 ph/subaperture/cycle and 1 ph/subaperture/cycle), where it seems to outperform both FriM and MVM. This means that fainter objects could be used as natural guide stars with the FTR.

Comparing the parallelized MVM algorithm with the "black-box" FTR algorithm did not give a large difference in latency, but comparing it with the parallelized FTR algorithm presents a completely different scenario. The parallelized FTR algorithm is 30 times faster than the MVM, for the 210x210 subapertures case. It is even faster when using several processors. The FTR algorithm has been implemented for parallel processing, by several research groups using different architectures. The parallelized Fourier Transform Reconstruction has been performed already at the required 5 ms limit[1] using two different computer architectures: Graphics Processing Units and Field Programmable Gate Arrays. Marichal-Hernández et al.[7] have been able of recovering the wavefront from gradient estimates for problems of size 256x256 within 5 ms using Graphics Processing Units, and J. M. Rodríguez-Ramos et al.[11] have achieved to perform a 256x256 2D FFT within 0.93 ms using Field Programmable Gate Arrays.

Future work will be focused on several aspects. We plan to study the performance of the FTR for SCAO using the modified Hudgin filter with the Shack-Hartmann geometry. The Hudgin filter is not blind to waffle so it should give a better performance, and it should converge faster, as we have already seen in our local simulations. We will also continue the tests for the application of the FTR to GLAO. As we have explained in Section 5, when using only one processor the first 2 direct FFT's can be parallelized, and what increases the latency is the fact of calculating the entire inverse FFT. Using several processors should decrease this latency, and we will continue our work in this direction. Also, we want to study the application of the algorithm to the multi-conjugate AO case. We plan to use the Fourier Slice Theorem in order to reconstruct the atmospheric volume. This theorem has been extensively studied in Computerized Tomography[12, 13], and the process is equivalent to a weighted back-propagation[14]. It consists on reconstructing "slices" of atmosphere parallel to the guide star direction, taking 1D-FFT's of the different projections to build a 2D Fourier space that is inverse-transformed to build the reconstructed slice[15]. Since there are a finite number of projections, we need to use the available information relative to the atmosphere we are reconstructing, C_n2, to weight the inverse-transforms and obtain a better estimate, as it is done in the case of weighted back-propagations[16].

ACKNOWLEDGEMENTS

We would like to thank Clèmentine Bèchet for her very useful hints that help us to do the simulations presented in this work. This project forms part of the ELT Design Study and is supported by the European Commission, within Framework Programme 6.

REFERENCES

[1] L. A. Poyneer, D. T. Gavel, and J. M. Brase, "Fast wave-front reconstruction in large adaptive optics systems with use of the Fourier transform," Journal of the Optical Society of America A, 19, 2100-2111 (2002).

[2] C. Béchet, M. Tallon, and E. M. Thiébaut, "Performances of the fractal iterative method with an internal model control law on the ESO end-to-end ELT adaptive optics simulator " Proc. SPIE. 7015.

[3] I. M. Hook, [The science case for the European Extremely Large Telescope: The next step in mankind's quest for the Universe], (2005).

[4] K. R. Freischlad, and C. L. Koliopoulos, "Modal estimation of a wave front from difference measurements using the discrete Fourier transform," Journal of the Optical Society of America A, 3, 1852-1861 (1986).

[5] M. Le Louarn, C. Vérinaud, V. Korkiakoski *et al.*, "Adaptive optics simulations for the European Extremely Large Telescope," Proc. SPIE. 6272, 98.

[6] E. Chu, and A. George, [Inside the FFT Black Box, Serial and Parallel Fast Fourier Transform Algorithms] CRC Press, London(2000).
[7] J. G. Marichal-Hernández, J. M. Rodríguez-Ramos, and F. Rosa, "Modal Fourier wavefront reconstruction using Graphics Processing Units," Journal of Electronic Imaging, 16(2), 023005 (2007).
[8] C. Correia, [Fourier-domain reconstructor for SCAO. Open and closed-loop simulations] European Southern Observatory (2006).
[9] H. J. Nussbaumer, [Fast Fourier Transform and Convolution Algorithms] Springer-Verlag, Berlin(1982).
[10] J. D. Markel, "FFT-pruning," IEEE Trans. Audio Electracoust, 19, 305-311 (1971).
[11] J. M. Rodríguez-Ramos, E. Magdaleno, C. D. Conde *et al.*, "2D-FFT implementation on FPGA for wavefront phase recovery from the CAFADIS camera," Proc. SPIE. 7015-116.
[12] H. Choi, and D. C. Munson, "Direct-Fourier reconstruction in tomography and synthetic aperture radar," International Journal of Imaging Systems and Technology, 9, 1-13 (1998).
[13] A. C. Kak, and M. Slaney, [Principles of Computerized Tomographic Imaging] IEEE Press, (1988).
[14] D. Gavel, and j. Milovich, "Tomographic reconstruction for multi-guidestar adaptive optics."
[15] D. Zosso, M. Bach Cuadra, and J.-P. Thiran, "Direct Fourier Tomographic Reconstruction Image-To-Image Filter," The Insight Journal, July-December, (2007).
[16] D. T. Gavel, "Tomography for multiconjugate adaptive optics systems using laser guide stars," Proc. SPIE. 5490, 1356-1373.